Mapping stellar kinematics across the Galactic bar

Kozlowski, S.; Wozniak, P. R.; Mao, S.; Smith, M. C.; Sumi, T.; Vestrand, W. T.; Wyrzykowski, L.

Published in:
Monthly Notices of the Royal Astronomical Society

DOI:
10.1111/j.1365-2966.2006.10487.x

Publication date:
2006

Mon. Not. R. Astron. Soc. **370,** 435–443 (2006) doi:10.1111/j.1365-2966.2006.10487.x

Mapping stellar kinematics across the Galactic bar: *HST* measurements of proper motions in 35 fields⋆

S. Kozłowski,[1]† P. R. Woźniak,[2] S. Mao,[1] M. C. Smith,[3] T. Sumi,[4] W. T. Vestrand[2] and Ł. Wyrzykowski[5]

[1]*Jodrell Bank Observatory, The University of Manchester, Macclesfield, Cheshire SK11 9DL*
[2]*Los Alamos National Laboratory, MS-D466, Los Alamos, NM 87545, USA*
[3]*Kapteyn Institute, PO Box 800, 9700 AV Groningen, the Netherlands*
[4]*Princeton University Observatory, Princeton, NJ 08544, USA*
[5]*Institute of Astronomy, University of Cambridge, Madingley Road, Cambridge CB3 OHA*

Accepted 2006 April 26. Received 2006 April 26; in original form 2006 March 22

ABSTRACT

We present a proper motion mini-survey of 35 fields in the vicinity of Baade window, $(l, b) = (1^\circ, -4^\circ)$, sampling roughly a 5×2.5-deg^2 region of the Galactic bar. Our second epoch observations collected with the Advanced Camera for Surveys/High Resolution Channel instrument onboard the *Hubble Space Telescope* were combined with the archival Wide Field Planetary Camera 2/PC images. The resulting time baselines are in the range of 4 to 8 yr. Precise proper motions of 15 863 stars were determined in the reference frame defined by the mean motion of stars with magnitudes between $I_{F814W} = 16.5$ and 21.5 along the line of sight. We clearly detect small gradients in proper motion dispersions (σ_l, $\sigma_b \sim (3.0, 2.5)$ mas yr^{-1}, and in the amount of anisotropy ($\sigma_l/\sigma_b \sim 1.2$). Both the longitude dispersion σ_l and its ratio to the vertical motion σ_b increase towards the Galactic plane. The decline of the anisotropy ratio σ_l/σ_b towards the minor axis of the bulge is mostly due to increasing σ_b. We also find, for the first time, a significant negative covariance term in the transverse velocity field $\sigma_{lb}/(\sigma_l\sigma_b) \simeq -0.10$. Our results extend by a factor of $\sim$15 the number of the Galactic bar fields with good proper motion dispersions.

Key words: gravitational lensing – Galaxy: bulge – Galaxy: disc – Galaxy: kinematics and dynamics.

1 INTRODUCTION

The Milky Way appears to be a typical spiral galaxy with a disc and bulge. While our unique inside view of the Galaxy helps to understand the Galactic structure in general, it also makes it more difficult to identify structures such as bars. The case for the existence of a bar at the Galactic centre – first proposed by de Vaucouleurs (1964) – is easier to make knowing that bars are common in external galaxies.

There is now conclusive evidence that the Galactic bulge is of a barred type. The longitude asymmetry of the *COBE* photometric maps (Blitz & Spergel 1991; Dwek et al. 1995), high optical depths to gravitational microlensing (Zhao, Spergel & Rich 1995), asymmetric star counts (Stanek et al. 1994; Babusiaux & Gilmore 2005), non-circular gas kinematics (de Vaucouleurs 1964), and triaxiality of the stellar velocity field (Zhao, Spergel & Rich 1994; Zhao, Rich & Biello 1996) have all been interpreted as signatures of the Galactic bar. Unfortunately, the size and precise orientation of the bar are still being debated. Recently Benjamin et al. (2005) found that the infrared star counts collected by the *Spitzer Space Telescope* are best explained assuming a bar with a half-length 4.4 ± 0.5 kpc placed at an angle of $\sim$44° to the Sun–Galactic centre line. Most previous studies prefer a bar at $\sim$20° extending out to $\sim$3.5 kpc (e.g. Gerhard 2001). Such apparently conflicting evidence may be an indication that the inner Galaxy hides even more complicated structures. A secondary bar (Alard 2001; Babusiaux & Gilmore 2005) and a ring (Sevenster & Kalnajs 2001) have been suggested, since these features are also evident in many other spiral galaxies (e.g. Erwin & Sparke 1999).

Binney (2005) discussed the progress of the dynamical modelling techniques in the context of major observational advances

⋆Based on observations made with the NASA/ESA *Hubble Space Telescope*, obtained from the data archive at the Space Telescope Science Institute (STScI). The STScI is operated by the Association of Universities for Research in Astronomy, Inc., under NASA contract NAS 5-26555.

†E-mail: simkoz@jb.man.ac.uk

Table 1. Log of the *HST* observations.

MACHO field	RA	Dec.	First epoch				Second epoch	
			Year	*F814W* exposure (s)	*F555W* exposure (s)	Proposal ID	Year	*F814W* exposure (s)
108-C	18:00:01.276	−28:27:41.23	1996.82	6 × 260		6756	2005.16	4 × 260
119-C	18:03:03.010	−30:09:56.50	1996.82	6 × 260		6756	2005.15	4 × 260
119-D	18:04:24.825	−30:05:58.94	1996.82	6 × 260		6756	2004.78	4 × 260
120-A	18:07:26.441	−29:39:34.22	1996.82	6 × 260		6756	2005.15	4 × 260
167-A	18:13:32.154	−26:31:10.33	1996.82	6 × 260		6756	2005.16	4 × 260
101-C	18:07:32.649	−27:31:35.60	1997.47	6 × 260		6756	2005.15	4 × 260
95-BLG-11. . .	18:04:37.239	−30:12:11.45	1996.67	6 × 260		6756	2005.16	4 × 260
96-BLG-17. . .	18:06:09.107	−27:53:38.59	1996.81	6 × 260		6756	2005.17	4 × 260
119-A.	18:03:35.789	−29:42:01.26	1996.68	6 × 160	2 × 400	6756	2005.14	4 × 160
95-BLG-7. . . .	18:13:29.298	−26:13:58.12	1998.84	2 × 40	3 × 40	7431	2005.46	4 × 40
95-BLG-10 . .	17:58:16.011	−29:32:10.86	1997.82	2 × 40	3 × 40	7431	2004.66	4 × 40
95-BLG-13 . .	18:08:47.038	−27:40:47.25	1999.45	2 × 40	3 × 40	7431	2005.12	4 × 40
95-BLG-14 . .	18:01:26.308	−28:31:14.03	2000.45	2 × 40	3 × 40	7431	2005.40	4 × 40
95-BLG-19 . .	18:11:32.487	−27:45:26.99	1998.49	2 × 40	3 × 40	7431	2005.44	4 × 40
97-BLG-18 . .	18:03:15.254	−28:00:14.06	1998.59	2 × 40	3 × 40	7431	2005.31	4 × 40
104-C	18:03:34.050	−28:00:18.94	1998.73	2 × 40	3 × 40	7431	2005.43	4 × 40
104-D	18:03:29.024	−28:00:30.99	1998.80	2 × 40	3 × 40	7431	2005.45	4 × 40
108-A	18:00:25.866	−28:02:35.24	1998.80	2 × 40	3 × 40	7431	2005.16	4 × 40
128-B	18:07:18.624	−28:59:29.83	1998.49	2 × 30	3 × 40	7431	2005.37	4 × 30
104-B	18:03:09.046	−28:01:45.25	1999.45	2 × 40	3 × 40	7431	2005.39	4 × 40
128-A	18:06:57.621	−29:00:55.15	1999.33	2 × 40	3 × 40	7431	2005.49	4 × 40
94-BLG-3 . . .	17:58:25.300	−29:47:59.50	1997.82	2 × 40	3 × 40	7431	2005.48	4 × 40
94-BLG-4 . . .	17:58:36.766	−30:02:19.27	1997.82	2 × 40	3 × 40	7431	2005.16	4 × 40
95-BLG-36 . .	18:07:20.775	−27:24:09.69	1998.80	2 × 40	3 × 40	7431	2005.39	4 × 40
95-BLG-37 . .	18:04:34.452	−28:25:33.46	1999.43	2 × 40	3 × 40	7431	2004.67	4 × 40
95-BLG-38 . .	17:59:41.851	−28:12:10.31	1998.81	2 × 40	3 × 40	7431	2005.33	4 × 40
95-BLG-41 . .	18:02:06.332	−28:50:45.26	1999.46	2 × 40	3 × 40	7431	2005.44	4 × 40
96-BLG-14 . .	18:05:15.421	−27:58:25.01	1997.83	2 × 40	3 × 40	7431	2004.67	4 × 40
96-BLG-4 . . .	18:06:11.954	−28:16:52.77	1998.79	2 × 26	3 × 40	7431	2004.82	4 × 26
97-BLG-38 . .	18:04:06.083	−27:48:26.25	1998.51	2 × 40	3 × 40	7431	2004.63	4 × 40
97-BLG-24 . .	18:04:20.253	−27:24:45.28	1998.35	2 × 40	3 × 40	7431	2005.49	4 × 40
96-BLG-5 . . .	18:05:02.497	−27:42:17.23	1999.45	4 × 160	2 × 400	8490	2005.12	4 × 160
98-BLG-6 . . .	17:57:32.812	−28:42:45.41	2000.48	2 × 100	2 × 260	8654	2004.73	4 × 100
97-BLG-41 . .	17:56:20.691	−28:47:41.97	2000.47	4 × 100	4 × 160	8654	2004.62	4 × 100
99-BLG-22 . .	18:05:05.281	−28:34:41.69	2001.77	4 × 400	4 × 400	9307	2005.16	4 × 400

expected from a future space mission *GAIA*. The three approaches to constructing a self-consistent dynamical Galaxy model are the Schwarzschild method (Zhao et al. 1994; Häfner et al. 2000), the torus modelling method (see Binney 2005 for details) and N-body simulations with particle weights determined by the 'made-to-measure' algorithm (Syer & Tremaine 1996). The first Galactic bar model employing the latter method was built by Bissantz, Debattista & Gerhard (2004). Neither of these techniques can fully address the structure of the inner Galaxy without constraints on stellar kinematics. The refinement of the models is limited largely by the scarcity of good proper motion and radial velocity measurements. Bissantz et al. (2004), for example, compared kinematic predictions of their model with the data for just two lines of sight. A handful of samples published since the pioneering photographic work of Spaenhauer, Jones & Whitford (1992) is not enough to remove the non-uniqueness of the model parameters.

In a study based on two lines of sight, Kuijken & Rich (2002) had demonstrated that high-quality relative proper motions can be obtained with a relatively modest investment of time using the *Hubble Space Telescope* (*HST*). At the resolution of the Wide Field Planetary Camera 2 (WFPC2) instrument, the required time baseline is only a few years. The *HST* archive contains a number of images suitable as the first epoch data, so the tedious part of accumulating the baseline can be avoided entirely. Most of these fields are centred around microlensing events discovered by the massive compact halo object (MACHO) collaboration (e.g. Popowski et al. 2005). Using a similar concept to that of Kuijken & Rich (2002), we carried out a mini-survey of proper motions in 35 of the available MACHO fields to study the kinematics of microlensed sources and of the general stellar populations. Here, we present the measurement techniques and results for the general stellar population in these 35 lines of sight.

2 *HST* IMAGES AND DATA REDUCTION

The log of the *HST* observations used in our proper motion mini-survey is given in Table 1. The first epoch images (selected from the *HST* archive)[1] were all taken with the WFPC2/PC camera, and cover the time interval 1996–2000. The second epoch data come from our own SNAP programme (cycle 13; proposal ID 10198) and were collected in 2004 and 2005 using the High Resolution Channel (HRC) of the Advanced Camera for Surveys (ACS). Our SNAP survey was optimized towards high execution rates and, therefore,

[1] http://archive.stsci.edu/hst/.

we only requested *F814W* observations to keep the required target visibility as low as possible. Both the PC and HRC detectors cover a similar field of view (25×29 and 35×35 arcsec^2, respectively) and have comparable pixel scales (27 versus 45.5 mas). There were no restrictions on the telescope roll angle during ACS observing. While the latter relaxed condition decreased the number of possible proper motion determinations, it greatly improved scheduling opportunities. Most of the subsequent analyses for each of the 35 fields are based on a pair of good-quality *F814W* (*I*-band) images constructed by stacking all suitable data for a given epoch. In some cases, the first epoch data included *F555W* (*V*-band) images that allowed us to construct colour–magnitude diagrams (CMDs). We also re-analysed the two fields previously studied by Kuijken & Rich (2002), increasing to 37 the total number of the Galactic bulge fields considered here.

2.1 Image reductions

The basic reductions of the ACS images, that is, de-biasing, dark frame subtraction, flat-fielding, and cosmic-ray removal, were performed on the fly by the standard *HST* data-processing pipeline. This pipeline also takes care of dithering, cosmic-ray splits and geometric corrections using the MULTIDRIZZLE software (Koekemoer et al. 2002), which in turn uses the DRIZZLE routines (Fruchter & Hook 2002). Our ACS observations employed a generous four-point dithering pattern combined with a two-way cosmic-ray split, providing the final DRIZZLEd images with high signal-to-noise ratio (S/N), excellent dynamic range and highly reliable cosmic-ray rejection. In the case of the first epoch WFPC2 images, we utilized the standard *HST* data products for individual exposures, and then used the DRIZZLE task of the IRAF package to correct the geometric distortions. For cosmic-ray cleaning, registering and combining these corrected images, we developed dedicated IRAF scripts. The quality of our final cross-instrument astrometry is limited by the larger pixel size, as well as the lower S/N and number of the individual first epoch PC frames available for stacking by comparison to the ACS data (see Section 3).

2.2 Object catalogues and point spread function fitting

The instrumental positions and magnitudes of the field objects were measured using the IRAF task STARFIND, an improved version of DAOFIND that fits Gaussian profiles to stellar images. The combined images from both the WFPC2/PC and ACS/HRC detectors have a well-sampled point spread function (PSF) with the full width at half-maximum (FWHM) of stellar images, respectively, 2.4 and 2.8 pixels. Our PSF fits were restricted within the area of the Airy disc (3.0 and 2.0 pixel radius for PC and HRC data, respectively), where the point-source flux is well approximated by a Gaussian model. Outside the Airy disc, the PSFs show a variety of shapes, including rings, possible diffraction spikes and bright spots in the case of high-S/N objects. These features can mimic stars and need to be carefully considered during object cross-identification. We imposed a minimum separation of $3 \times$ FWHM between any two sources detected in the same image to ensure that there are essentially no spurious objects in the final source lists. The loss of number statistics due to the accidental rejection of the actual stars in tight groups is insignificant. In fact, the centroid measurements for objects in the wings of other stars are notoriously unreliable and best avoided. The minimum separation cut also helps in cross-identification of objects between the two epochs (Section 3), since the expected intrinsic object shifts may reach $\sim$2 PC pixels.

The final object catalogues were converted to the VEGA magnitude system (Girardi et al. 2002, and references therein) and the astrometric transformations to the Galactic (l, b) coordinates were established using the World Coordinate System (WCS) headers of the ACS images. Our estimated S/Ns for object fluxes are based on propagated errors in pixel counts that account for photon statistics.

3 ESTIMATING TRANSVERSE MOTIONS OF THE GALACTIC BULGE STARS

Absolute astrometry is difficult in the crowded Galactic bulge fields. Until we can establish a sample of extragalactic objects (e.g. spectroscopically confirmed quasi-stellar objects in the catalogue of candidates by Sumi et al. 2005) shining through the low-extinction windows, the only readily available reference velocity in the Galactic bulge is the mean velocity of stars along the line of sight. Note, however, that the second-order moments of proper motions are unaffected by the choice of our reference frame. In this analysis, we use the magnitude- and distance-selected samples to investigate the spatial dependence of the covariance matrix of the transverse velocity field across the Galactic bar.

3.1 Relative proper motions and their dispersions

Having measured the instrumental positions of stars on both the first and second epoch images, we tied the WFPC2/PC positions to the ACS/HRC pixel grid. The object shifts Δl and Δb in the Galactic coordinates between the two epochs could then be calculated using the WCS information from the ACS headers. We cross-correlated the positions of a few hundred stars in the magnitude range $16.5 < I_{F814W} < 21.5$ to obtain the coordinate transformation between two pixel grids, which is approximated by a third-order polynomial. Stars brighter than $I_{F814W} = 16.5$ were often saturated while those with $I_{F814W} > 21.5$ were too faint to have useful S/Ns, particularly for the fields with short exposures (Table 1). Our procedure for cross-identifying stars starts from matching the first 20 objects (out of $\sim$50 brightest stars with $17 < I_{F814W} < 18$) using the triangle algorithm (Groth 1986; Woźniak 2000). The initial low-order fit is then iteratively refined. A star with a transverse velocity of 100 km s^{-1} at the distance of 8 kpc will move by 26.4 mas, or roughly one ACS/HRC pixel, assuming a 10-yr baseline. Accordingly, we adopted a tolerance radius of 100 mas for the final matching.

After geometrically aligning and transforming object positions to the Galactic (l, b) coordinates, we folded the data with the time baseline and estimated all components of the transverse velocity tensor, that is, dispersions σ_l, σ_b and the normalized covariance $C_{lb} \equiv \sigma_{lb}/(\sigma_l \sigma_b)$. The sample of stars used to trace the kinematic parameters of the Galactic bulge was limited to the magnitude range $18.0 < I_{F814W} < 21.5$, that is, dominated by the bulge main-sequence population near the turn-off point. This puts all lines of sight (with data sets of the varying depth and dynamic range) on a more common footing. However, as already noted by Kuijken & Rich (2002), the results are insensitive to the details of the magnitude cuts.

3.2 Astrometric errors

The 1σ centroid errors from PSF fitting (per coordinate) can be estimated from the S/N:

$$\delta \simeq \gamma \times \frac{\mathrm{FWHM}}{\mathrm{S/N}}, \qquad (1)$$

where $\gamma = 0.6$ for a Gaussian PSF model and the FWHM is in pixels (see e.g. Kuijken & Rich 2002). We tested this prescription by stacking independent subsets of images taken at a single epoch. Similarly to Kuijken & Rich (2002), we find that equation (1) is an excellent representation of the actual astrometric uncertainties in our data, with the exception of the brightest stars, for which a constant systematic contribution of 0.025 pixel is required. Consequently, we used equation (1) with the systematic term added in quadrature to estimate the astrometric errors and their contribution to the apparent proper motion dispersions. The formulae for estimating σ_l, σ_b and their errors corrected for the measurement variance can be found in Spaenhauer et al. (1992). Throughout this paper, we use bootstrapped uncertainties of the sample statistics (from 1000 trials) that turned out to be slightly more conservative than analytical formulae. The estimated intrinsic dispersions reported in Section 4 are 5–10 per cent lower compared to the raw values. The cross-term C_{lb} need not be corrected, as long as the errors in l and b are uncorrelated. None of our conclusions depends on the precise value or even the presence of this correction.

The limiting S/N for a useful detection in our analysis is about 10 and corresponds to an $I_{F814W} \simeq 21.5$ mag star in the combined image of two 40-s WFPC2/PC exposures. The same star will be detected at S/N $\sim$ 20 in the lowest-quality ACS stack (four 40-s frames). The shortest time baseline in our data is 3.388 yr, and the typical 1σ astrometric uncertainties for a 21.5-mag star are $\sim$7.2 and $\sim$2.1 mas in the first and second epoch images, respectively. In this worst-case scenario, the proper motion can be measured to an accuracy of 2.5 mas yr^{-1}. The images for the first eight fields in Table 1 have relatively long exposure times, so the resulting proper motion errors are only $\sim$0.1 mas yr^{-1} for bright stars and $\sim$0.3 mas yr^{-1} for the faintest stars in those samples, with a systematic error of 0.025 pixel (cf. discussion following equation 1).

4 RESULTS

The results are given in Table 2 and plotted in Figs 1 and 2. Proper motions for individual stars are available online.[2] After presenting our measurements, we check for consistency with two other published data sets (Section 4.3). A more detailed discussion and comparison to the results of Kuijken & Rich (2002) follows in Section 5.

4.1 Proper motion dispersions

The spatial dependence of proper motion dispersions σ_l, σ_b is shown in Fig. 1. Recall that at a distance of 8 kpc, a velocity of 100 km s^{-1} implies a proper motion of 2.64 mas yr^{-1}. The most visible trends are in $\sigma_l(b)$ and $\sigma_b(l)$ that tend to increase closer to the Galactic plane and Galactic centre. Both gradients are weak, but clearly present. From a simple straight line fit we find

$$\sigma_l = 0.16 \pm 0.04 \times b + 3.38 \pm 0.13, \quad (2)$$

$$\sigma_b = -0.09 \pm 0.02 \times l + 2.62 \pm 0.06. \quad (3)$$

Consequently, σ_b increases from 2.1 to 2.6 mas yr^{-1}, or by about 20 per cent, as the longitude l varies from $5\overset{\circ}{.}5$ to $0\overset{\circ}{.}5$. Similarly, σ_b changes from 2.6 to 3.2 mas yr^{-1} between $b = -4\overset{\circ}{.}5$ and -2°. It is intriguing that the last data point around $b \approx -2^\circ$ has the lowest dispersion (σ_l) measured for all fields (see the top right-hand panel in Fig. 1), but the value is still marginally consistent with the observed scatter. There is no other indication of the intrinsic variations on the field-to-field scale. The distributions of $\sigma_l(l)$ and $\sigma_b(b)$ are flat within the scatter from random errors and projection effects in the presence of gradients.

[2] http://www.jb.man.ac.uk/~simkoz/dispersions/.

4.2 Anisotropy and covariance

In Fig. 2, we plot the ratio and the correlation coefficent (covariance of the velocity field) of σ_l and σ_b as a function of location in the bulge. There is a significant level of anisotropy, that is, $\sigma_l/\sigma_b > 1$, throughout the covered area. Moreover, the velocity distribution shows a tendency to become more isotropic for lines of sight approaching the Galactic centre at a roughly fixed latitude b. This is a reflection of the increase in σ_b with approximately constant σ_l (Section 4.1). The trend of more anisotropy towards the Galactic plane is also driven primarily by one of the dispersions (σ_l), but it is more difficult to see. Part of the reason for this is the narrow range of b covered by the data. The formal fits give

$$\sigma_l/\sigma_b = 0.05 \pm 0.01 \times l + 1.08 \pm 0.03, \quad (4)$$

$$\sigma_l/\sigma_b = 0.03 \pm 0.03 \times b + 1.27 \pm 0.08. \quad (5)$$

The estimates of the covariance term from Table 2 (plotted in Fig. 2) are all negative and scatter uniformly in the range $-0.20 < C_{lb} < -0.02$. This indicates that in our Galactic bulge fields the stellar motions in directions parallel and perpendicular to the plane are significantly anticorrelated. An observational bias that would account for this anticorrelation has to operate in a similar way over a large range of instrumental settings. For example, a serious concern is a presence of preferred telescope orientations. Indeed, for about half of our fields the relative roll angle between the two compared observations falls in a narrow range of 25°. The other half, however, is spread over all possible orientations and still shows about the same covariance. The skewness of the ACS focal plane cannot be the cause of the observed correlation, because the measurements in both Kuijken & Rich (2002) fields use only WFPC2/PC data and yet they perfectly agree with the rest of the C_{lb} values. We also investigated several other possibilities; we found no explanation for this result other than a true correlation between μ_l and μ_b. Taking a field with a relatively low S/N in our data and assuming perfectly correlated errors in μ_l and μ_b, the expected covariance is only $C_{lb} \sim 0.02$. There is a slight hint in Fig. 2 that C_{lb} may vary with the longitude, although this impression seems to rely on the two points farthest from the bulge minor axis ($l \simeq 5\overset{\circ}{.}3$ in the left-hand panel of Fig. 2) that fall below the rest of the data.

4.3 Comparisons with previous work

4.3.1 OGLE-II proper motion catalogue

Sumi et al. (2004) used large number statistics of the OGLE-II data base (Udalski, Kubiak & Szymański 1997) to derive relative proper motions of $\gtrsim 5 \times 10^6$ stars in the Galactic bulge region from hundreds of observations covering a 4-yr baseline. The OGLE-II catalogue is a valuable resource for kinematic studies of bright stars like red clump giants that are relatively free of the source confusion effects. However, at the 1.3-arcsec-FWHM seeing of the ground-based OGLE-II images, a random red clump giant star still has a few per cent probability of being blended with another unresolved star. It is instructive to cross-validate the results of Sumi et al. (2004) and our high-resolution *HST* measurements against each other.

Table 2. Results of our proper motion mini-survey. The dispersions σ_l, σ_b and the dimensionless correlation coefficient C_{lb} were measured for 35 lines of sight in the Galactic bulge (l, b). The time baseline Δt and the number of stars $N_{\rm stars}$ used to estimate the kinematics are also given.

Field name	l (°)	b (°)	σ_l (mas yr^{-1})	σ_b (mas yr^{-1})	C_{lb}	Δt (yr)	$N_{\rm stars}$
101-C	3.65	−3.47	2.85 ± 0.09	2.45 ± 0.08	−0.15 ± 0.05	7.683	445
104-B	2.73	−2.87	2.97 ± 0.10	2.50 ± 0.10	−0.05 ± 0.05	5.941	407
104-C	2.80	−2.93	2.74 ± 0.09	2.51 ± 0.10	−0.15 ± 0.04	6.706	482
104-D	2.79	−2.92	2.84 ± 0.10	2.36 ± 0.10	−0.10 ± 0.05	6.649	437
108-A	2.42	−2.35	2.90 ± 0.12	2.32 ± 0.12	−0.08 ± 0.06	6.360	396
108-C	2.02	−2.48	3.15 ± 0.10	2.52 ± 0.07	−0.09 ± 0.04	8.345	615
119-A	1.32	−3.77	2.89 ± 0.10	2.44 ± 0.08	−0.14 ± 0.04	8.458	471
119-C	0.85	−3.89	2.79 ± 0.10	2.65 ± 0.08	−0.14 ± 0.04	8.339	459
119-D	1.06	−4.12	2.75 ± 0.10	2.56 ± 0.09	−0.05 ± 0.06	7.962	420
120-A	1.76	−4.48	2.75 ± 0.09	2.52 ± 0.09	−0.04 ± 0.05	8.339	397
128-A	2.28	−4.08	2.63 ± 0.11	2.33 ± 0.12	−0.12 ± 0.05	6.165	357
128-B	2.33	−4.13	2.70 ± 0.12	2.29 ± 0.13	−0.13 ± 0.06	6.881	338
167-A	5.17	−4.16	2.75 ± 0.11	2.36 ± 0.09	−0.18 ± 0.05	8.345	317
94-BLG-3 ...	0.68	−2.84	2.84 ± 0.10	2.58 ± 0.10	−0.12 ± 0.05	7.654	496
94-BLG-4 ...	0.49	−3.00	2.58 ± 0.11	2.46 ± 0.09	−0.03 ± 0.04	7.341	413
95-BLG-10 ...	0.89	−2.68	3.07 ± 0.10	2.41 ± 0.09	−0.12 ± 0.04	6.840	487
95-BLG-11 ...	0.99	−4.21	2.82 ± 0.09	2.62 ± 0.09	−0.14 ± 0.04	8.493	443
95-BLG-13 ...	3.64	−3.78	2.61 ± 0.13	2.31 ± 0.12	−0.14 ± 0.05	5.672	309
95-BLG-14 ...	2.12	−2.78	2.95 ± 0.13	2.50 ± 0.11	−0.12 ± 0.05	4.950	463
95-BLG-19 ...	3.87	−4.36	2.61 ± 0.11	2.17 ± 0.10	−0.13 ± 0.06	6.952	300
95-BLG-36 ...	3.73	−3.37	2.75 ± 0.12	2.11 ± 0.11	−0.10 ± 0.05	6.587	376
95-BLG-37 ...	2.54	−3.33	2.72 ± 0.12	2.44 ± 0.12	−0.04 ± 0.05	5.238	442
95-BLG-38 ...	2.20	−2.29	2.87 ± 0.12	2.46 ± 0.10	−0.05 ± 0.04	6.526	474
95-BLG-41 ...	1.91	−3.07	2.79 ± 0.10	2.34 ± 0.10	−0.04 ± 0.05	5.980	450
95-BLG-7	5.42	−4.01	2.86 ± 0.14	1.88 ± 0.11	−0.20 ± 0.07	6.616	265
96-BLG-14 ...	3.01	−3.24	2.71 ± 0.12	2.40 ± 0.12	−0.17 ± 0.05	6.833	373
96-BLG-17 ...	3.17	−3.38	3.07 ± 0.10	2.55 ± 0.09	−0.16 ± 0.04	8.364	557
96-BLG-4	2.84	−3.57	2.68 ± 0.14	2.26 ± 0.14	−0.04 ± 0.06	6.027	329
96-BLG-5	3.22	−3.07	3.17 ± 0.10	2.39 ± 0.08	−0.13 ± 0.05	5.670	535
97-BLG-18 ...	2.77	−2.87	2.99 ± 0.10	2.38 ± 0.10	−0.12 ± 0.04	6.713	433
97-BLG-24 ...	3.40	−2.79	3.00 ± 0.11	2.39 ± 0.10	−0.10 ± 0.05	7.115	398
97-BLG-38 ...	3.03	−2.94	2.95 ± 0.12	2.21 ± 0.10	−0.06 ± 0.05	6.118	395
97-BLG-41 ...	1.32	−1.95	2.58 ± 0.07	2.13 ± 0.07	−0.09 ± 0.04	5.145	612
98-BLG-6	1.53	−2.13	3.26 ± 0.10	2.79 ± 0.12	−0.07 ± 0.05	4.252	670
99-BLG-22 ...	2.46	−3.50	3.11 ± 0.10	2.60 ± 0.09	−0.17 ± 0.04	3.388	493
KR-BW[a]	1.14	−3.77	2.87 ± 0.08	2.59 ± 0.08	−0.07 ± 0.03	6.048	694
KR-SgrI	1.26	−2.66	3.07 ± 0.08	2.73 ± 0.07	−0.09 ± 0.04	5.960	752

[a]KR-BW and KR-SgrI are the Baade window and the Sagittarius-I field, respectively, from Kuijken & Rich (2002).

Out of the 35 programme fields in Table 1, 15 are covered by the OGLE-II proper motion catalogue. In our *HST* sample, we found 77 stars for which the OGLE-II catalogue proper motion error is $\leqslant$3 mas yr^{-1}. The two data sets were compared star by star after adjusting for an arbitrary zero-point of the proper motion scale. The results are plotted in Fig. 3 and show a good overall agreement of our measurements with Sumi et al. (2004). All significant outliers were labelled and checked for blending. Fig. 4 demonstrates that virtually all these substantial discrepancies are linked to the presence of an unresolved companion within ∼1 arcsec of the primary object.

4.3.2 Kuijken & Rich (2002)

Our approach to measuring the positions and proper motions of stars (Section 2.2) is somewhat simpler than the method used by Kuijken & Rich (2002). The latter study utilized the images from the WFPC2/WF chips and had to accommodate a strong undersampling of the PSF. In contrast, our use of the WFPC2 data was limited to the critically sampled images from the PC detector. The second epoch ACS/HRC images have four times the PSF sampling of the WF images, so we could take advantage of the conventional PSF fitting techniques.

Regardless, in order to eliminate the possibility of a hidden error we re-analysed the PC data in both fields studied by Kuijken & Rich (2002) using our tools. Table 3 shows the results of this comparison. The agreement between the two sets of measurements is remarkably close despite significant differences in the sample size and the adopted selection criteria. This also confirms that our results are not significantly affected by several subtle instrumental effects that can potentially influence astrometric work with the *HST* images (e.g. Kuijken & Rich 2002 and references therein).

5 DISCUSSION

5.1 Distance and population trends

The study of Kuijken & Rich (2002) focused on cleaning the Galactic bulge population and removing the contamination by the bluer disc

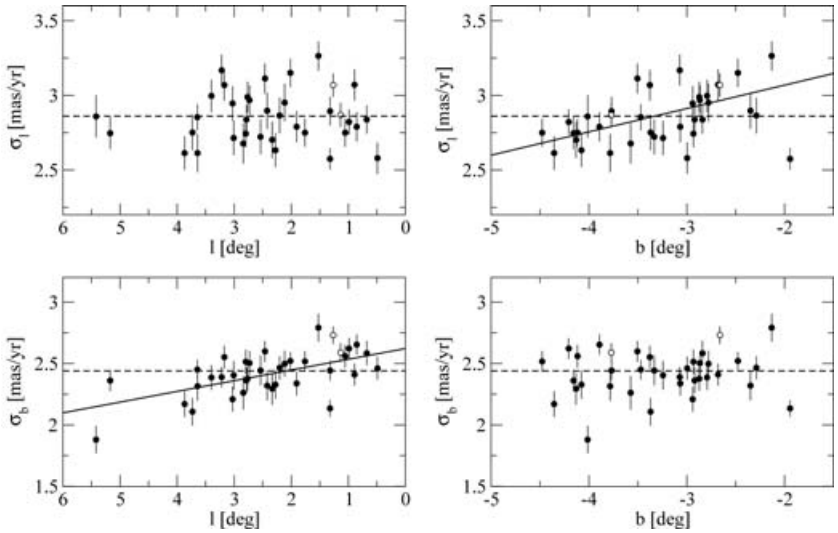

Figure 1. Spatial dependence of proper motion dispersions σ_l and σ_b in the Galactic coordinates for our turn-off point dominated sample in the Galactic bulge (Table 2 and Section 4). The two open circles are for the Baade window and Sagittarius-I fields from Kuijken & Rich (2002). The lines show linear regressions (solid) and weighted means (dashed) of the data. For the top right-hand panel, the rightmost data point was not used in the fit.

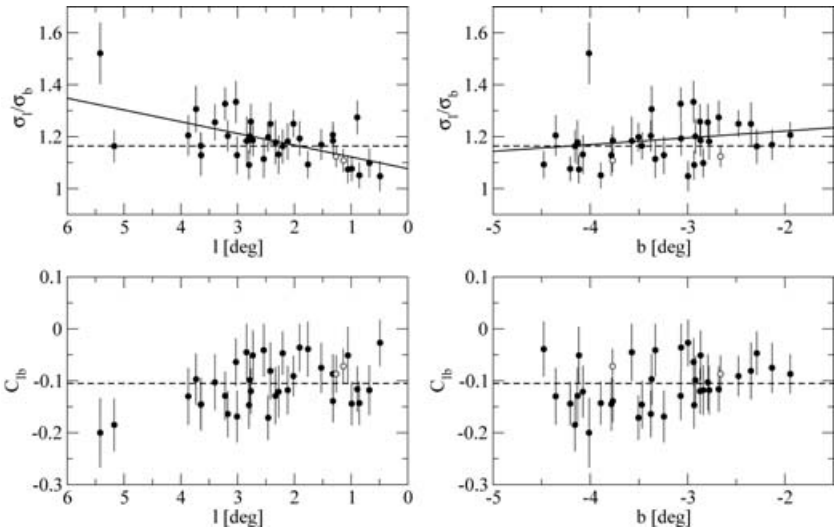

Figure 2. Similar to Fig. 1 but for the anisotropy ratio σ_l/σ_b and covariance term $C_{lb} \equiv \sigma_{lb}/(\sigma_l \sigma_b)$.

stars. Above the bulge turn-off point, the stellar colours alone are sufficient to separate the blue disc main sequence from the red giants, subgiants and clump giants. The size of our fields is generally too small to provide useful statistics of bright stars above turn-off point, and good colour information is only available for about a third of the lines of sight. However, three of the fields in Table 1 with useful colours (97-BLG-18, 104-C and 104-D) are close to each other and were combined in order to look for a kinematic distinction between the Galactic disc and bulge populations. Figs 5 and 6 show that in the frame of reference of a mean star (of any colour), the longitude proper motions of the blue disc stars are biased towards positive values, while the red bulge stars tend to have more negative μ_l. The blue and red samples were selected, correspondingly, using conditions $(V - I) < 1.65$ and $(V - I) > 1.7$. This effect was previously observed by Sumi et al. (2005) and by Kuijken & Rich (2002) in their two fields with multiepoch WFPC2 data and there is little doubt that it is due to the blue disc stars 'rotating in front' of the red bulge stars.

Kuijken & Rich (2002) also devised an approximate distance measure

$$M^* = I_{F814W} - 2(V_{F555W} - I_{F814W}) \quad (6)$$

chosen to remove the slope of the main sequence in the CMD. In Fig. 7, we present the average proper motions and their dispersions for the Baade window in bins of M^*. As expected, with an increasing depth along the line of sight, the kinematic signature gradually changes from that characteristic of the disc stars, to the one typical for the bulge. In the Kuijken & Rich (2002) data, this trend continues to very faint stars that are likely on the far side of the bulge, and if so, it constitutes a 'rotation curve' of the bulge. The colours for our

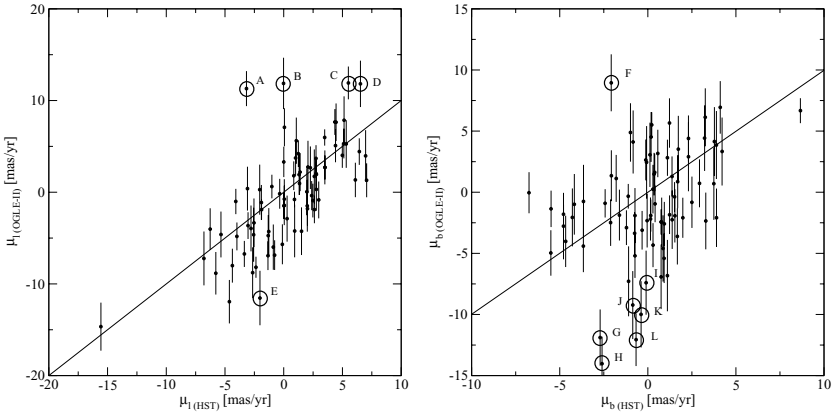

Figure 3. Comparison between our *HST* measurements and the ground-based OGLE-II data for bright stars from the catalogue of Sumi et al. (2004). There are 77 stars covered by our observations that have catalogue errors 3 mas yr^{-1} or better in Sumi et al. Significant discrepancies (marked by the alphabets) are caused by blending (cf. Fig. 4). The solid lines indicate that the two measurements (ground-based OGLE-II and *HST*) are equal.

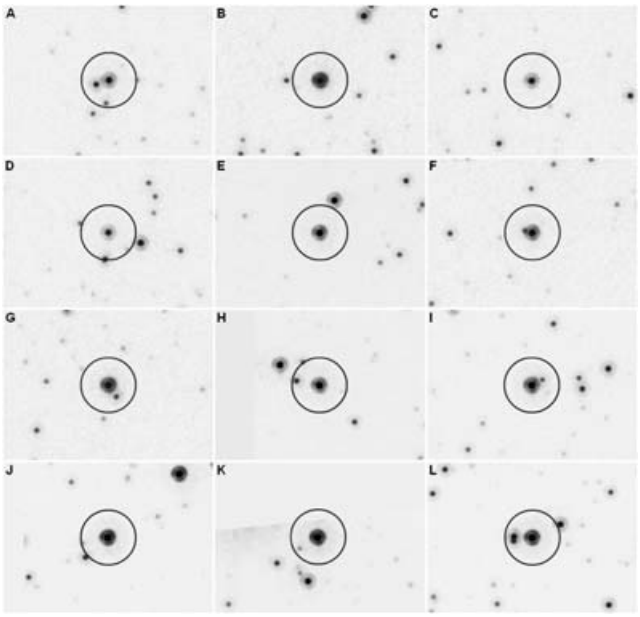

Figure 4. Cut-out *HST* images for the outliers marked by alphabets in Fig. 3. All significant outliers in Fig. 3 can be linked to source confusion and flux blending. The dark circles have a diameter of 1 arcsec.

fields are generally of lower S/N or non-existent, and do not allow to see this much detail.

5.2 Stellar velocity ellipsoid of the Galactic bar

A detailed modelling of the measurements in Table 2 is beyond the scope of this paper. Here we only comment on possible directions and new possibilities.

Zhao et al. (1996) interpreted the bulge anisotropy in terms of the rotation support of the Galactic bulge and related the ratio σ_l/σ_b directly to the level of flattening of the light density distribution. They also concluded that the value $\sigma_l/\sigma_b = 1.10$–1.15 observed in Baade window $(l, b) \sim (1^\circ, -4^\circ)$, with which our measurements are consistent, can be explained by rigid rotation. The presence of any disc stars, however, will also contribute rotational broadening to σ_l. Since in the vicinity of our fields the disc fraction increases closer to the plane, it follows that the measured gradient from equation (2) could be due to the disc contamination. The changes of skewness in the μ_l distribution tend to support this (see Fig. 6). Another possibility is that the rotation rate of the bulge actually increases at lower $|b|$, as found by Izumiura et al. (1995) from the radial velocities of 124 SiO masers in the Galactic bulge. It has been observed that for giants in Baade window the metal-poor stars display more spread in the vertical motion and less anisotropy when compared to metal-rich samples (Zhao et al. 1994, 1996). Both metallicity dependencies are quite steep, so it is likely that the gradient from equation (3) is related to a changing mix of populations with more metal-poor stars closer to the Galactic bulge minor axis.

We are not aware of any previous detections of the cross-terms in the Galactic bulge velocity field except the report by Zhao et al. (1994) of a significant vertex deviation between the radial and longitudinal motions from C_{rl}. That result is based on a photographic sample of ∼200 K and M giants from Spaenhauer et al. (1992). We note that the latter sample actually shows a hint of a slightly negative covariance between μ_l and μ_b (cf. fig. 1 of Zhao et al. 1994). The superb resolution of the *HST* enabled very significant detections of the C_{lb} cross-term in many fields. The non-diagonal elements of the velocity tensor are crucial to determining the dominant orbit families, the importance of streaming motions and the need for the intrinsic anisotropy versus solid body rotation in the Galactic bulge (Zhao et al. 1994, 1996; Häfner et al. 2000). Häfner et al. (2000)

Table 3. Proper motion dispersions from Kuijken & Rich (2002) compared with the results of our re-analysis of the same data.

Field	l	b	This work			Kuijken & Rich (2002)		
			σ_l	σ_b	N_{stars}	σ_l	σ_b	N_{stars}
BW	1.14	−3.77	2.87 ± 0.08	2.59 ± 0.08	694	2.91 ± 0.06	2.51 ± 0.05	1076
Sgr-I	1.27	−2.66	3.07 ± 0.08	2.73 ± 0.07	752	3.10 ± 0.06	2.73 ± 0.05	1388

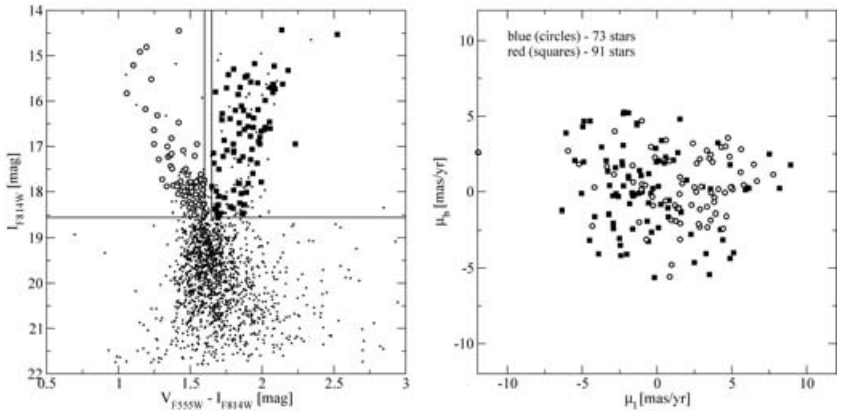

Figure 5. CMD (left-hand panel) and relative proper motions (right-hand panel) for stars in three nearly coincident stellar fields from Table 2: 97-BLG-18, 104-C and 104-D. The red (squares) and blue (circles) stars above the turn-off point show the kinematic characteristics of the bulge and disc populations, respectively.

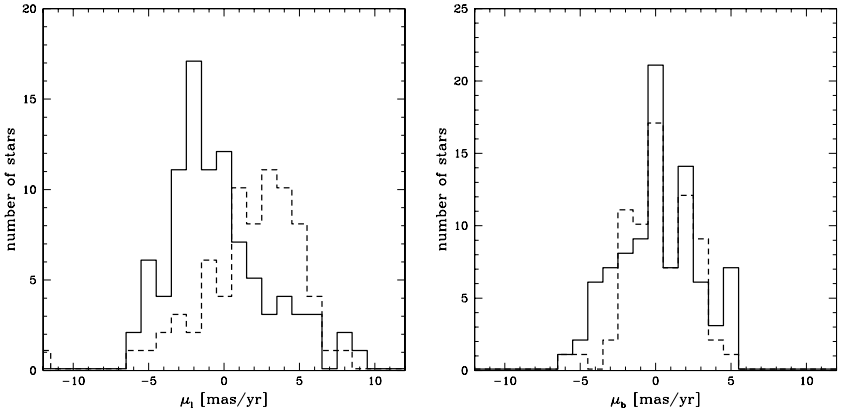

Figure 6. Histograms of relative proper motions of the red (solid line) and blue (dashed line) samples from Fig. 5 The blue disc stars 'rotate in front' of the Galactic bulge parallel to the plane.

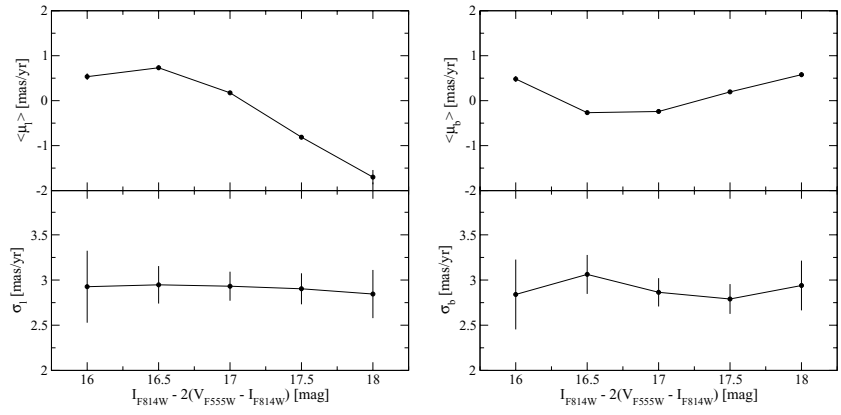

Figure 7. Average relative proper motions and dispersions of stars in the Baade Window in bins of $M^* \equiv I_{F814W} - 2 \times (V_{F555W} - I_{F814W})$, an approximate distance indicator.

published detailed calculations of C_{lb} for several lines of sight at positive longitudes including Baade window ($1^\circ, -4^\circ, C_{lb} = 0.04$), and two others: ($8\overset{\circ}{.}4, -6^\circ, C_{lb} = 0.15$) and ($1\overset{\circ}{.}21, -1\overset{\circ}{.}67, C_{lb} = 0.04$). Taken at face value, these predictions are roughly of the same magnitude as the results from Section 4, but have the opposite sign. For a proper comparison with dynamical models like the ones in Häfner et al. (2000) and Bissantz et al. (2004), we need to wait until the calculations are folded with the appropriate selection functions,

since our measurements are based on substantially deeper data than most of the previous samples.

6 SUMMARY AND CONCLUSIONS

The main results of our proper motion mini-survey are: (1) high-quality proper motion measurements for hundreds of stars in 35 lines of sight across the Galactic bar, (2) establishing the presence of spatial gradients in dispersions σ_l, σ_b and the amount of anisotropy σ_l/σ_b, and (3) the first reliable detection of the covariance term C_{lb} of the transverse velocity tensor. We cross-validated our measurements with the ground-based OGLE-II data of Sumi et al. (2004) and a benchmark study of Kuijken & Rich (2002). The observed slow rise of σ_l towards the Galactic plane is likely due to the increasing disc contamination and/or a possible gradient in the bulge rotation speed. The increase in σ_b towards the minor axis of the bulge is accompanied by the decreasing ratio σ_l/σ_b and possibly results from increasing fraction of metal-poor stars. Another possibility is that σ_b increases due to the larger surface density of stars at low l (closer to the Galactic centre). We clearly detect the covariance term $C_{lb} \sim -0.10$ that implies a significant tilt of the Galactic bulge velocity ellipsoid with respect to the Galactic plane. Using the same procedures as in Binney & Merrifield (1998, Section 10.3.2), we find the tilt is roughly equal to -24°.

The data presented in this paper provide qualitatively new constraints on dynamical models of the inner Galaxy and dramatically improved number statistics. Furthermore, it may be possible in the near future to augment our proper motion samples with the distance and metallicity estimates. As shown by Kuijken & Rich (2002), deep CMDs can supply sufficiently accurate distance information to effectively isolate the bulge population. In order to maximize the discriminating power of model comparisons, the focus should be on extending the coverage to negative longitudes and locations farther from the Galactic centre.

ACKNOWLEDGMENTS

We thank Prof. Bohdan Paczyński, Prof. Ian Browne and Dr Vasily Belokurov, Dr Wyn Evans and Dr Nicholas Rattenbury for helpful comments.

Support to PRW for proposal SNAP-10198 was provided by NASA through a grant from the STScI, which is operated by the Association of Universities for Research in Astronomy, Inc., under NASA contract NAS5-26555.

This work was partly supported by the European Community's Sixth Framework Marie Curie Research Training Network Programme, Contract No. MRTN-CT-2004-505183 'ANGLES', in particular SK through a studentship, ŁW through a PDRA, and SM through travel support.

MCS acknowledges financial support from the Netherlands Organisation for Scientific Research (NWO).

REFERENCES

Alard C., 2001, A&A, 379, L44
Alcock C. et al., 2000, ApJ, 541, 734
Babusiaux C., Gilmore G., 2005, MNRAS, 358, 1309
Benjamin R. A. et al., 2005, ApJ, 630, L149
Binney J. J., 2005, 2005 Proc. Gaia Symp., preprint (astro-ph/0411229)
Binney J. J., Merrifield M. R., 1998, Galactic Astronomy. Princeton Univ. Press, Princeton, NJ
Bissantz N., Debattista V. P., Gerhard O., 2004, ApJ, 601, L155
Blitz L., Spergel D. N., 1991, ApJ, 379, 631
de Vaucouleurs G., 1964, in Kerr F., Rodgers A., eds, Proc. IAU Symp. 20, The Galaxy and the Magellanic Clouds. Australian Academy of Sciences, Canberra, p. 195
Dwek E. et al., 1995, ApJ, 445, 716
Erwin P., Sparke L. S., 1999, ApJ, 521, L37
Fruchter A. S., Hook R. N., 2002, PASP, 114, 144
Gerhard O., 2001, in Funes J. G., Corsini E. M. eds, ASP Conf. Ser. Vol. 230, Galaxy discs and disc Galaxies. Astron. Soc. Pac., San Francisco, p. 21
Girardi L., Bertelli G., Bressan A., Chiosi C., Groenewegen M. A. T., Marrigo P., Salasnich B., 2002, A&A, 391, 195
Groth E. J., 1986, AJ, 91, 1244
Häfner R., Evans N. W., Dehnen W., Binney J., 2000, MNRAS, 314, 433
Izumiura H. et al., 1995, ApJS, 98, 271
Koekemoer A. M., Fruchter A. S., Hook R. N., Hack W., The 2002 *HST* Calibration Workshop, 2002, 339
Kuijken K., Rich R. M., 2002, AJ, 124, 2054
Popowski P. et al., 2005, ApJ, 631, 879
Sevenster M. N., Kalnajs A. J., 2001, AJ, 122, 885
Spaenhauer A., Jones B. F., Whitford A. E., 1992, AJ, 103, 297
Stanek K. Z., Mateo M., Udalski A., Szymański M., Kaluzny J., Kubiak M., 1994, ApJ, 429, L71
Sumi T. et al., 2004, MNRAS, 348, 1439
Sumi T. et al., 2005, MNRAS, 356, 331
Syer D., Tremaine S., 1996, MNRAS, 282, 223
Udalski A., Kubiak M., Szymański M., 1997, Acta Astron., 47, 319
Woźniak P., 2000, Acta Astron., 50, 421
Zhao H. S., Spergel D. N., Rich R. M., 1994, AJ, 108, 2154
Zhao H. S., Spergel D. N., Rich R. M., 1995, ApJ, 440, L13
Zhao H. S., Rich R. M., Biello J., 1996, ApJ, 470, 506

This paper has been typeset from a TEX/LATEX file prepared by the author.